Project Number 282910

ÉCLAIRE

Effects of Climate Change on Air Pollution Impacts and Response Strategies for European Ecosystems

Seventh Framework Programme

Theme: Environment

D4.2 – Ozone dry deposition parameterisations: Ozone dry deposition parameterisations, improved with respect to changes in climate and environmental conditions, suitable for inclusion in CTMs

Due date of deliverable: **31/10/2014** Actual submission date: **03/11/2014**

Start Date of Project: **01/10/2011** Duration: **48 months**

Organisation name of lead contractor for this deliverable :
Stockholm Environment Institute-York, University of York

Project co-funded by the European Commission within the Seventh Framework Programme		
Dissemination Level		
PU	Public	X
PP	Restricted to other programme participants (including the Commission Services)	☐
RE	Restricted to a group specified by the consortium (including the Commission Services)	☐
CO	Confidential, only for members of the consortium (including the Commission Services)	☐

1. Executive Summary

Existing surface/atmosphere exchange models for O_3 were further developed and tested versus new ECLAIRE datasets to better represent ozone deposition to the ecosystem compartments and include responses to climate and environmental conditions: (1) stomatal deposition driven by photosynthesis; (2) cuticular deposition and (3) ground deposition. Three models served as basis for these developments and validations: the **DO3SE** model, with a focus on stomatal exchange and link with photosynthesis, the **SURFATM** model for testing new ground deposition parameterisation, and **MUSICA** for developing a new wet-cuticle deposition module.
New parameterisations have been developed and are ready for inclusion in ESX modelling framework: (1) A new stomatal uptake module including photosynthesis; (2) a wet cuticular deposition module as a function of total reaction rate in the water film; (3) a parameterisation of O_3 deposition to ground as a function of surface relative humidity. All these parameterisation have been tested against ECLAIRE or previously existing datasets.
A new DO3SE_C module has been incorporated into the DO_3SE model framework (essentially substituting the previous g_{sto} module, which used a multiplicative model to estimate g_{sto} based on Jarvis, 1976). The model has been parameterised for European land cover types, consistent with those used by the EMEP model. This has required the identification from the literature of 5 parameter values for 9 landcover types made up of 11 different species. Finally, the model has been coded so as to allow easy incorporation into the ESX modelling scheme.

Objectives:
To improve an existing ozone deposition model to include climate and environmental conditions changes suitable for inclusion in CTMs (DO3SE, Deposition of Ozone for Stomatal Exchange)

1. parameterisation of the model for application across Europe within the EMEP model and;
2. a model formulation coded so as to be easily available for use in EMEP (the ESX model).
3. Development and test of new parameterisation of ozone deposition to ground
4. Development and test of new parameterisation of ozone deposition to wet cuticle.

2. Activities:

- Literature review to parameterise the model for European conditions.
- Work on programming the code to identify the mechanisms by which these algorithms can be incorporated into the ESX model framework.
- Literature review on parameterisation of dry deposition of ozone to ground
- Literature review on dry deposition of ozone to the cuticle.
- Development of new module on ozone deposition to wet cuticle.

3. Results:

- Identification of the algorithms that will together form the new A_{net}-g_{sto} module
- Parameterisation of the model for European land cover types
- Coding of the new algorithms into the existing DO_3SE model (substituting the existing multiplicative algorithms)
- Parameterisation of ground ozone deposition as a function of surface relative humidity
- Parameterisation of ozone deposition to wet cuticles as a function of total water chemical reaction rate

4. Milestones achieved:

MS 15: Literature review on the effects of ozone and nitrogen deposition on stomatal functioning and on the influence of surface wetness on total O_3 deposition.
MS 17: Improved representation of the influence of environmental drivers on stomatal conductance

5. Deviations and reasons:

None

6. Publications:

Potier E. 2014. Modélisation de l'effet de la structure du couvert végétal et des réactions chimiques avec les oxydes d'azote et les composés organiques volatils biogéniques sur l'impact de l'ozone sur les écosystèmes terrestres. *PhD* thesis, University Marie-Curie (Paris 6), 132p (French. Including three papers in English).
Potier E., Jérôme Ogée Julien Jouanguy ; Eric Lamaud; Patrick Stella; Erwan Personne; Brigitte Durand; Nicolas Mascher and Benjamin Loubet, 2014. Multilayer modelling of ozone fluxes on winter wheat reveals large deposition on wet senescing leaves. *Agricultural and Forest Meteorol*. Accepted with major corrections.
Stella P., Personne E., Lamaud E., Loubet B., Trebs I., Cellier P., 2013. Assessment of the total, stomatal, cuticular, and soil 2 year ozone budgets of an agricultural field with winter wheat and maize crops. Journal of Geophysical Research - Biogeosciences, 118, 3, 1120–1132.

7. Meetings:

8. List of Documents/Annexes:

1- A new algorithm for ozone stomatal conductance including photosynthesis and ozone feedback
2- A new parameterisation of ozone fluxes to wet cuticles
3- A new parameterisation of ozone fluxes to the ground including air relative humidity

1. Ozone Dry Deposition Parameterisations

1. The new DO3SE_C model.

The objective of the coupled photosynthesis-stomatal conductance model (A_{net}-g_{sto}) model is to quantify leaf or canopy scale g_{sto} with the help of easily accessible environmental parameters such as air temperature (T_{air}), ambient CO_2 concentration (c_a) and irradiance (PAR). The A_{net}-g_{sto} model consists of a combination of two separate models, whose main components are outlined below and include i. the empirical A_{net}-g_{sto} model that estimates g_{sto} (Leuning, 1990) and ii. the mechanistic and biochemical Farquhar model (Farquhar et al., 1980) that estimates net carbon assimilation or net photosynthesis (A_{net}).

One of the first coupled A_{net}-g_{sto} models was that published by (Leuning, 1990), though some other authors are often cited as the originating sources of the model (e.g. Collatz et al., 1991 and Harley et al., 1992). The models they apparently developed independently are essentially equivalent. The order of description of the A_{net}-g_{sto} modelling here follows the order in which they have to be computed.

2. Parameterisation of the new DO3SE_C model

A literature review was conducted to parameterise the new model. This review focussed on the following key model parameters:

Jmax - Maximum photosynthetic electron transport rate (a proxy for ribulose-1,5-bisphosphate regeneration)
Vcmax - Maximum carboxylation rate of Rubisco
m - Species-specific composite sensitivity of gs to An,
g0 – minimum stomatal conductance

All values taken from the literature were measurements made at 25^{o}C to ensure the values were not affected by temperature variation (Medlyn et al., 2002).

These parameters were found for 9 land cover types (denoted in bold in Table 1) and within these cover types, 11 species. These species and cover-types are those already defined by the EMEP photochemical model and the original, multiplicative DO3SE model. Therefore, this parameterisation gave consistency with the existing methods used to estimate deposition and stomatal ozone flux across Europe.

3. Coding the new algorithms into the existing DO3SE model for availability to ESX

The ESX model provides a new method of estimating atmospheric and in canopy exchange of pollutants. The ESX scheme is not based on resistances but relies on numerically solving diffusion equations for different pollutants with a parameterised exchange coefficient; essentially these equations replace the atmospheric and boundary layer resistances previously in the EMEP and DO_3SE models. The benefit of this unique approach is that these models are able to estimate both downward and upward flux of pollutants (i.e. can cope with pollutants that are both deposited to- as well as emitted from- vegetation such as ammonia (NH_3)).

The ESX model includes a layer-based canopy framework, numerical solutions to pollutant dispersal and the EMEPs model atmospheric chemistry algorithms. Each layer contains pollutant sources and sinks (e.g. due to presence of vegetation), has chemical interactions calculated within it, and is affected by dispersal between layers (see Figure 1; where z_i relates to pollutant mass transfer either as a source (z_i+1) or a sink (z_i-1) from a pollutant concentration defined at z_i). The model is designed to run over a short time step to work within EMEP's larger scale chemical transport model.

Figure 1. A conceptualisation of the quantification of pollutant fluxes between layers within the ESX model.

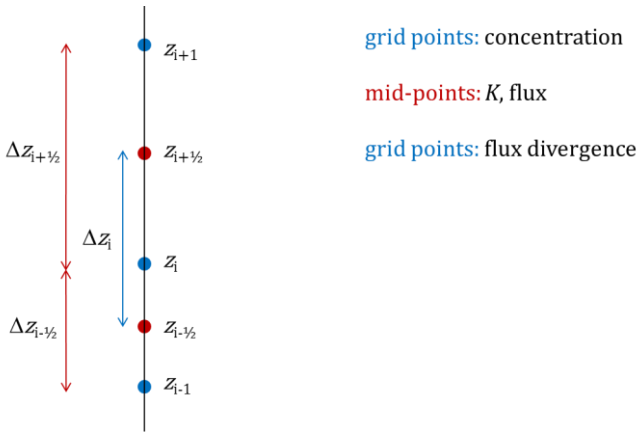

Table 1. Parameterisation of the DO3SE_C model – maximum carboxylation (Vcmax, µmol/m^2/s) and maximum photosynthetic electron transport rate (Jmax, µmol/m^2/s) (Jmax).

Species / cover type	Vcmax, µmol/m2/s (mean, median, range)	Ref	Jmax, µmol/m2/s (mean, median, range)	Ref
Deciduous forest	**56**	**N.B. JULES value is 36.8** (Clark et al., 2011)	**112**	
Birch	**51**, 57, [42-71]	Hayes, 2014 Pers. Comm. [57], Rey & Jarvis, 1998 [42], Dreyer, et al., 2001 [71]	**102**, 92, [84-125]	Hayes, 2014 Pers. Comm. [84], Rey & Jarvis, 1998 [92], Dreyer, et al., 2001 [125]
Beech	**52**, 52, [35-62]	Bader et al., 2010 [44], Löw et al., 2007 [62], Parelle et al., 2006 [50], Dreyer, et al., 2001 [66], Balandier et al., 2007 [35], Fleck, 2001 [55]	**107**, 107, [83-128]	Bader et al., 2010 [120], Löw et al., 2007 [113], Parelle et al., 2006 [98], Dreyer, et al., 2001 [128], Balandier et al., 2007 [83], Fleck, 2001 [100]
Temperate Oak	**65**, 69, [31-91]	Marzuoli & Gerosa (2014) Pers. Comm. [31], Dreyer et al., 2001 [88] & [91], Bader et al., 2010 [50]	**129**, 152, [57-157]	Marzuoli & Gerosa (2014) Pers. Comm. [57], Dreyer et al., 2001 [154] & [157], Bader et al., 2010 [150]
Coniferous forest	**79**	**N.B. JULES value is 26.4** (Clark et al., 2011)	**190**	
Norway spruce	**71**, 71, [60-81]	Zheng et al., 2002 [81], Niinemets, 2002 [60]	**162**, 162, [143-180]	Zheng et al., 2002 [180], Niinemets, 2002 [143]
Scots pine	**87**, 83, [38-144]	Niinemets et al., 2001 [48], Niinemets, 2002 [83], Warren et al., 2003 [123], Jach & Ceulemans, 2000 [144], Wang, 1996 [38]	**219**, 237, [110-345]	Niinemets et al., 2001 [110], Niinemets, 2002 [237], Warren et al., 2003 [259], Jach & Ceulemans, 2000 [345], Wang, 1996 [146]
Mediterranean broadleaf evergreen	**56**		**97**	
Holm Oak	**56**, 50, [36-87]	Martin StPaul et al., 2012 [87], Niinemets, 2002 [36] & [40], Juárez-lópez, et al., 2008 [61]	**97**, 91, [59-139]	Martin StPaul et al., 2012 [139], Niinemets, 2002 [65] & [72], Juárez-lópez, et al., 2008 [110]
Mediterranean needleleaf evergreen	**56**		**97**	
Aleppo pine	No species specific data – use Holm Oak as surrogate			
Temperate Crops				
Wheat	180 [25-261]	Cf. Büker et al., 2007	400 [87-522]	Cf. Büker et al., 2007
Mediterranean Crops*	**48**	**Clark et al., 2011 [48]**	**105**	**(assuming Vcmax and Jmax ratio is same as Wheat at 2.2)**
Maize*	48	Clark et al., 2011 [48]	105	(assuming Vcmax and Jmax ratio is

				same as Wheat at 2.2)
Root Crops	180 [25-261]	**See wheat**	400 [87-522]	**See wheat**
Potato	180 [25-261]	See wheat	400 [87-522]	See wheat
Vineyards	**100 [50-100]**	**Büker et al., 2007**	**225 [120-260]**	**Büker et al., 2007**
Grapevine	100 [50-100]	Büker et al., 2007	225 [120-260]	Büker et al., 2007
Grassland/Semi-natural/Med Scrub	**48**	**Clark et al., 2011 [48]**	**105**	**(assuming Vcmax and Jmax ratio is same as Wheat at 2.2)**

Table 2. Parameterisation of the DO3SE_C model –minimum stomatal conductance (g0, mol H_2O m^{-2} s^{-1}), the ratio of Vcmax:Jmax (where red denotes a ratio based on the mean values of Jmax and VCmax found in the literature as in Table 1) and species-specific composite sensitivity of gs to An (m),

Species / cover type	g0,	Ref	Vcmax:Jmax	Ref	m	Ref
Deciduous forest	**0.03**	**0.03**	**2**			
Birch	0.03	Büker et al., 2007	**2** 1.81, 1.76 [1.47-2.19]	Hayes (2014) Pers. Comm. [1.47], Rey & Jarvis, 1998 [2.19], Dreyer, et al., 2001 [1.76]	**8.6**	Hayes (2014) Pers. Comm. [8.6]
Beech	0.03	Büker et al., 2007	**2.05** 2.11, 1.95, [1.82-2.37]	Bader et al., 2010 [2.73], Löw et al., 2007 [1.82], Parelle et al., 2006 [1.96], Dreyer, et al., 2001 [1.94], Balandier et al., 2007 [2.37], Fleck, 2001 [1.83]	**8.6**	Birch value used as surrogate
Temperate oak	0.03	Use Beech value	**1.98** 2, 2.7, [1.73-3.0]	Marzuoli & Gerosa (2014) Pers. Comm. [1.82], Dreyer et al., 2001 [1.75] & [1.731], Bader et al., 2010 [3.00]	**8.6**	Birch value used as surrogate
Coniferous Forest			**2.4**		**9.2**	
Norway spruce	0.03	Use Beech value	**2.28** 2.3, 2.3, [2.22-2.38]	Zheng et al., 2002 [2.22], Niinemets, 2002 [2.38]	**9.2**	Nikolov & Zeller, 2003 [9.2]
Scots pine	0.03	Use Beech value	**2.52** 2.65, 2.40, [2.11-3.84]	Niinemets et al., 2001 [2.32], Niinemets, 2002 [2.86], Warren et al., 2003 [2.11], Jach & Ceulemans, 2000 [2.40], Wang, 1996 [3.84]	**9.2**	Nikolov & Zeller, 2003 [9.2]
Mediterranean broadleaf evergreen			**1.73**		**8.6**	
Holm Oak	0.03	Use Beech value	**1.73** 1.7, 2, [1.6-1.8]	Martin StPaul et al., 2012 [1.6], Juárez-lópez, et al., 2008 [1.8]	8.6	Birch value used as surrogate
Mediterranean			**1.73**		**8.6**	

needleleaf evergreen						
Aleppo pine	0.03	Use Beech value	No species specific data – use Holm Oak as surrogate			
Temperate Crops	**0.02**	**Büker et al., 2007**	**2.22**	**Büker et al., 2007**	**8.12**	**Büker et al., 2007**
Wheat	0.02	Büker et al., 2007	**2.22**	Büker et al., 2007	8.12	Büker et al., 2007
Mediterranean Crops*	**0.02**	**See wheat**	**2.22**	**Büker et al., 2007**	**8.12**	**Büker et al., 2007**
Maize*	0.02	See wheat	**2.22**	Büker et al., 2007	8.12	Büker et al., 2007
Root Crops	**0.02**	**See wheat**	**2.22**	**Büker et al., 2007**	**8.12**	**Büker et al., 2007**
Potato	0.02	See wheat	**2.22**	Büker et al., 2007	8.12	Büker et al., 2007
Vineyards	**0.05**	**See wheat**	**2.25**	**Büker et al., 2007**	**6.14**	**Büker et al., 2007**
Grapevine	0.05	Büker et al., 2007	**2.25**	Büker et al., 2007	6.14	Büker et al., 2007
Grassland/Semi-natural/Med Scrub	**0.02**	**See wheat**	**2.22**	**Büker et al., 2007**	**8.12**	**Büker et al., 2007**

DO_3SE fits into this scheme by providing a sophisticated approach to calculating stomatal fluxes, and therefore pollutant exchange with the vegetation, in each of the canopy layers. Stomatal conductance is calculated on a per-layer basis using both general meteorological data and per-layer values resulting from the dispersal model (e.g. CO_2 concentration) and other canopy-related effects (e.g. attenuation of sunlight).

4. Development of the Fortran coding of the ESX-DO_3SE model

ESX can be described as a one-dimensional chemical transport model, working on a vertical grid, for a single land cover type. EMEP also has vertical transport within its larger 3-dimensional scheme, in addition to the large-scale horizontal grid and for several land covers per grid square. The EMEP model also uses several nested time intervals, most notably daily, 3-hourly, hourly and 20 minutes. As a smaller-scale model, ESX is run for every 20-minute interval, and every appropriate land cover, to solve the localised diffusion and chemical interactions. It is initialised with a starting state from the EMEP model's chemical concentrations data for the vertical range that ESX is being run for, and resulting fluxes are fed back to this data.

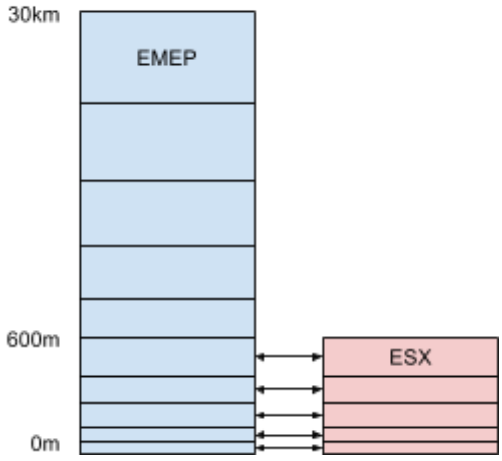

Figure 2. Scheme of the vertical grid spacing in ESX and EMEP

The existing code included much of the diffusion and chemical mechanism models (the latter being re-used from EMEP). A framework was created within which the various parts of the ESX-DO_3SE model could reside, i.e. the data flow between meteorological inputs, chemical concentrations, the diffusion model and DO_3SE's stomatal conductance model. An important aspect of this integration was to establish how to compromise on the design of both DO_3SE and ESX to allow ESX's version of DO_3SE to easily be updated with the most recent DO_3SE model developments without re-integration being a major undertaking each time changes were made to the DO_3SE model.

Similar considerations were needed to establish how to write ESX code that could be a standalone prototype but also be called from EMEP code. This required organising data variables within the model, grouping them where appropriate to give a coherent picture of flow within the model and making the code more maintainable. The DO_3SE model needed to be re-designed to allow it to be called from ESX code without hard-to-debug side-effects and without invoking aspects of the DO_3SE model that were in contradiction to the ESX model. This decoupling of DO_3SE methods from each other and the ESX model allowed improvements in this area to be tested within DO_3SE, ESX and EMEP with much less effort than before. This work has resulted in the production of a standalone ESX proof of concept model that could be driven by meteorological data, run a chemical interaction scheme and solve the diffusion model for vertical transport.

The integration of the new DO_3SE code into the ESX code has ensured that both multiplicative- and photosynthetic-based stomatal conductance methods to be configured and used by ESX. Code for the soil moisture part of the DO_3SE model was also integrated (for further details of this module see (Büker et al., 2012). Some additional work was required here to support the modelling of soil water content within ESX. Since ESX was already using some code duplicated from EMEP, ESX was converted to a "sub-project" of EMEP's codebase and a lot of duplication was removed, this allows easier maintainability and integration with EMEP.

The EMEP model runs several nested time loops, and in the innermost loop, deposition is calculated for each land use category. As a starting point, we chose this part of the model to call ESX, driving it with the data available at this stage, and recording the results, without feeding them back into EMEP. This allows the behaviour of ESX to be analysed without introducing any feedback-driven anomalies.

5. Conclusions

A new parameterisation of the stomatal uptake of ozone that included photosynthesis and zone impacts was developed and tested. The code was incorporated in ESX. Full details are given in deliverable D4.3.

6. References

Aphalo, P.J., & Jarvis, P. G. (1993). An analysis of Ball's empirical model of stomatal conductance. *Annals of Botany*, *72*, 312–327.

Bader, M. K.-F., Siegwolf, R., & Körner, C. (2010). Sustained enhancement of photosynthesis in mature deciduous forest trees after 8 years of free air CO(2) enrichment. *Planta*, *232*(5), 1115–25. doi:10.1007/s00425-010-1240-8

Balandier, P., Sinoquet, H., Frak, E., Giuliani, R., Vandame, M., Descamps, S., … Curt, T. (2007). Six-year time course of light-use efficiency, carbon gain and growth of beech saplings (Fagus sylvatica) planted under a Scots pine (Pinus sylvestris) shelterwood. *Tree Physiology*, *27*(8), 1073–1082. doi:10.1093/treephys/27.8.1073

Baldocchi, D. (1994). An analytical solution for coupled leaf photosynthesis and stomatal conductance models. *Tree Physiology*, *14*(7-8-9), 1069–1079. doi:10.1093/treephys/14.7-8-9.1069

Ball, J.T., Woodrow, I.E. Berry, J. A. (1987). A model predicting stomatal conductance and its contribution to the control of photosynthesis under different environmental conditions. In J. Biggens (Ed.), *Progress in photosynthesis research, Vol IV*. Dordrecht: Martinus Nijhoff.

Bernacchi, C. J., Singsaas, E. L., Pimentel, C., Portis Jr, a. R., & Long, S. P. (2001). Improved temperature response functions for models of Rubisco-limited photosynthesis. *Plant, Cell and Environment*, *24*(2), 253–259. doi:10.1046/j.1365-3040.2001.00668.x

Brooks, G.D., & Farquhar, A. (1985). Effect of temperature on the CO2/O2 specificity of ribulose-1,5-bisphosphate carboxylase/ oxygenase and the rate of respiration in light. *Planta*, *165*, 397–406.

Büker, P., Emberson, L. D., Ashmore, M. R., Cambridge, H. M., Jacobs, C. M. J., Massman, W. J., … de la Torre, D. (2007). Comparison of different stomatal conductance algorithms for ozone flux modelling. *Environmental Pollution (Barking, Essex : 1987)*, *146*(3), 726–35. doi:10.1016/j.envpol.2006.04.007

Clark, D. B., Mercado, L. M., Sitch, S., Jones, C. D., Gedney, N., Best, M. J., … Cox, P. M. (2011). The Joint UK Land Environment Simulator (JULES), model description – Part 2: Carbon fluxes and vegetation dynamics. *Geoscientific Model Development*, *4*(3), 701–722. doi:10.5194/gmd-4-701-2011

Collatz, G.J., Ball, J.T., Grivet, C. and Berry, J. A. (1991). Physiological and environmental regulation of stomatal conductance , photosynthesis and transpiration : a model that includes a laminar boundary layer *. *Agricultural and Forest Meteorology*, *54*(1074), 107–136.

Cox, P. M., Betts, R. a., Bunton, C. B., Essery, R. L. H., Rowntree, P. R., & Smith, J. (1999). The impact of new land surface physics on the GCM simulation of climate and climate sensitivity. *Climate Dynamics*, *15*(3), 183–203. doi:10.1007/s003820050276

Dreyer, E., Le Roux, X., Montpied, P., Daudet, F. A., & Masson, F. (2001). Temperature response of leaf photosynthetic capacity in seedlings from seven temperate tree species. *Tree Physiology*, *21*(4), 223–232. Retrieved from http://treephys.oxfordjournals.org/cgi/content/long/21/4/223

Farquhar, G.D., von Caemmerer, S., Berry, J. A. (1980). A biochemical model of photosynthetic CO2 assimilation in leaves of C3 species. *Planta*, *149*, 78–90.

Fleck, S. (2001). Integrated analysis of relationships between 3D-structure , leaf photosynthesis , and branch transpiration of mature Fagus sylvatica and Quercus petraea trees in a mixed forest stand, (August).

Harley, P. C., Thomas, R. B., Reynolds, J. F., & Strain, B. R. (1992). Modelling photosynthesis of cotton grown in elevated CO2. *Plant, Cell and Environment*, *15*(3), 271–282. doi:10.1111/j.1365-3040.1992.tb00974.x

Harley, P.C., Tenhunen, J.D., and Lange, O. L. (1986). Use of an analytical model to study limitations on net photosynthesis in Arbutus unedo under field conditions. *Oecologia*, *70*, 393–401.

Jach, M. E., & Ceulemans, R. (2000). Effects of season, needle age and elevated atmospheric CO2 on photosynthesis in Scots pine (Pinus sylvestris). *Tree Physiology*, *20*(3), 145–157. doi:10.1093/treephys/20.3.145

Juárez-lópez, F. J., Escudero, A., & Mediavilla, S. (2008). Ontogenetic changes in stomatal and biochemical limitations to photosynthesis of two co-occurring Mediterranean oaks differing in leaf life span, (1980), 367–374.

Kosugi, Y., Shibata, S., Kobashi, S., & Caemmerer, V. (2003). Parameterization of the CO2 and H2O gas exchange of several temperate deciduous broad-leaved trees at the leaf, 285–301.

Leuning, R. (1990). MODELING STOMATAL BEHAVIOR AND PHOTOSYNTHESIS OF EUCALYPTUS-GRANDIS. *AUSTRALIAN JOURNAL OF PLANT PHYSIOLOGY*, *17*(2), 159–175.

Leuning, R. (1995). A critical appraisal of a combined stomatal-photosynthesis model for C3 plants. *Plant, Cell and Environment*, *18*(4), 339–355. doi:10.1111/j.1365-3040.1995.tb00370.x

Leuning, R. (2002). Temperature dependence of two parameters in a photosynthesis model. *Plant, Cell and Environment*, 1205–1210.

Löw, M., Häberle, K.-H., Warren, C. R., & Matyssek, R. (2007). O3 flux-related responsiveness of photosynthesis, respiration, and stomatal conductance of adult Fagus sylvatica to experimentally enhanced free-air O3 exposure. *Plant Biology (Stuttgart, Germany)*, *9*(2), 197–206. doi:10.1055/s-2006-924656

Martin StPaul, N.K., Limousin, J.-M., Rodríguez-calcerrada, J., Ruffault, J., Rambal, S., Letts, M.G., Misson, L. (2012). Photosynthetic sensitivity to drought varies among populations of Quercus ilex along a rainfall gradient. *Functional Plant Biology*, *39*(39), 25–37.

Martin, M J., Farage, P.K., Humphries, S.W., and Long, S. P. (2000). Australian Journal of Plant Physiology. *Australian Journal of Plant Physiology*, *27*, 211–219.

Medlyn, B. E., Dreyer, E., Ellsworth, D., Forstreuter, M., Harley, P. C., Kirschbaum, M. U. F., … Loustau, D. (2002). Temperature response of parameters of a biochemically based model of photosynthesis. II. A review of experimental data. *Plant, Cell and Environment*, *25*(9), 1167–1179. doi:10.1046/j.1365-3040.2002.00891.x

Medlyn, B. E., Duursma, R. a., Eamus, D., Ellsworth, D. S., Prentice, I. C., Barton, C. V. M., … Wingate, L. (2011). Reconciling the optimal and empirical approaches to modelling stomatal conductance. *Global Change Biology*, *17*(6), 2134–2144. doi:10.1111/j.1365-2486.2010.02375.x

Niinemets, U. (2002). Stomatal conductance alone does not explain the decline in foliar photosynthetic rates with increasing tree age and size in Picea abies and Pinus sylvestris. *Tree Physiology*, *22*(8), 515–535. doi:10.1093/treephys/22.8.515

Niinemets, U., Ellsworth, D. S., Lukjanova, a., & Tobias, M. (2001). Site fertility and the morphological and photosynthetic acclimation of Pinus sylvestris needles to light. *Tree Physiology*, *21*(17), 1231–1244. doi:10.1093/treephys/21.17.1231

Nikolov, T., Massman, W.J., & Schoettle, A. W. (1995). Coupling biochemical and biophysical processes at the leaf level : an equilibrium photosynthesis model for leaves of C 3 plants. *Ecological Modelling*, *80*, 205–235.

Parelle, J., Roudaut, J.P., Ducrey, M. (2006). Light acclimation and photosynthetic response of beech (Fagus sylvatica L .) saplings under artificial shading or natural Mediterranean conditions. *Annals of Forest Science*, *63*, 257–266. doi:10.1051/forest

Rey, A., & Jarvis, P. G. (1998). Long-term photosynthetic acclimation to increased atmospheric CO concentration in young birch (Betula pendula) trees, (1996).

Sellers, P. J., Berry, J. A., Collatz, G. J., Field, C. B., & Hall, F. G. (1992). Canopy reflectance, photosynthesis, and transpiration. III - A reanalysis using improved leaf models and a new canopy integration scheme.

Remote Sensing of Environment, *42*(3), 187–216. Retrieved from http://linkinghub.elsevier.com/retrieve/pii/003442579290102P

Sellers, P.J., Randall. D.A., Collatz, G.J., Berry, J.A., Field, C.B., Dazlich, D.A., Zhang, C., Collelo, G.D. and Bounoua, L. (1996). A revised land surface parameterisation (SiB2) for atmospheric GCMs. Part I. Model formulation. *Journal of Climate*, *9*, 676–705.

Sharkey, T. D., Bernacchi, C. J., Farquhar, G. D., & Singsaas, E. L. (2007). Fitting photosynthetic carbon dioxide response curves for C(3) leaves. *Plant, Cell & Environment*, *30*(9), 1035–40. doi:10.1111/j.1365-3040.2007.01710.x

Su, H.-B., Paw U, K. T., & Shaw, R. H. (1996). Development of a coupled leaf and canopy model for the simulation of plant-atmosphere interaction. *Journal of Applied Meteorology*, *35*, 733–748. Retrieved from http://journals.ametsoc.org/doi/pdf/10.1175/1520-0450(1996)035<0733:DOACLA>2.0.CO;2

Von Caemmerer, S. & Farquhar, G. D. (1981). Some relationships between the biochemistry of photosynthesis and the gas exchange of leaves. *Planta*, *153*, 376–387.

Wang, K. (1996). Acclimation of photosynthetic parameters in Scats pine after three years exposure to elevated temperature and CO ,, *1923*(96).

Wang, Y., & Leuning, R. (1998). A two-leaf model for canopy conductance , photosynthesis and partitioning of available energy I : Model description and comparison with a multi-layered model. *Agricultural and Forest Meteorology*, *91*, 89–111.

Warren, C. R., Dreyer, E., & Adams, M. A. (2003). Photosynthesis-Rubisco relationships in foliage of Pinus sylvestris in response to nitrogen supply and the proposed role of Rubisco and amino acids as nitrogen stores, 359–366. doi:10.1007/s00468-003-0246-2

Wohlfahrt, G., Bahn, M., Haubner, E., Horak, I., Michaeler, W., Rottmar, K., … Cernusca, a. (1999). Inter-specific variation of the biochemical limitation to photosynthesis and related leaf traits of 30 species from mountain grassland ecosystems under different land use. *Plant, Cell and Environment*, *22*(10), 1281–1296. doi:10.1046/j.1365-3040.1999.00479.x

Wullschleger, S. D. (1993). Biochemical Limitations to Carbon Assimilation in C 3 Plants — A Retrospective Analysis of the j Curves from 109 Species. *Journal of Experimental Botany*, *44*(262), 907–920.

Zheng, D., Freeman, M., Bergh, J., Røsberg, I., & Nilsen, P. (2002). Production of Picea abies in South-east Norway in Response to Climate Change: A Case Study Using Process-based Model Simulation with Field Validation. *Scandinavian Journal of Forest Research*, *17*(1), 35–46. doi:10.1080/028275802317221064

2. A new parameterisation of ozone fluxes to wet cuticles

1. Modelling water film layers in a multi-layer model

Canopy rain interception and water storage on leaf surfaces are computed in each vegetation layer using a water balance equation and the concept of maximum storage capacity (Rutter *et al.*, 1971). The leaf fraction covered with liquid water in vegetation layer j ($p_{wet,j}$) is then computed from the corresponding water storage ($W_{f,j}$, kg m^{-2} of ground area) as:

$$_{wet,leaf} = \left(\frac{W_f}{W_{f,max}}\right)^{\mu} \quad (1)$$

Where $W_{f,max,j}$ (kg m^{-2} of ground area) denotes the maximum water storage capacity of vegetation layer j (assumed proportional to leaf area, i.e., $W_{f,max,j} = W_{f,max}L_j$) and μ is a parameter related to the wettability of the leaf cuticle, ranging from 0 (full wettability) to 1 (constant thickness). When condensation occurs Eq. 1 is replaced by $p_{wet,j} = 1$, assuming that dew forms on the entire leaf surface. Evaporation from wet leaves is weighted by $p_{wet,j}$ to account for the actual evaporating surface. For the purpose of this study and in order to model ozone deposition on wet leaves canopy water storage $W_{f,j}$ was converted into a water film thickness ($l_{w,j}$) as follows:

$$l_{w,j} = \frac{W_{f,j}/\rho_w}{L_j p_{wet,j}} \quad (2)$$

Where ρ_w is the water density and L_j (m^2 m^{-2} of ground area) is the leaf area of the j_{th} vegetation layer (*j* is used in the following to design the layer number). Finally, for representation purposes only, a mean canopy-scale water film thickness (l_w) was computed as:

$$l_w = \frac{\sum L_j p_{wet,j} l_{w,j}}{\sum L_j p_{wet,j}} \quad (3)$$

2. Ozone deposition scheme to wet cuticles

Leaf conductance for ozone on wet cuticles was modelled physic-chemically-based: accounting for ozone solubility in water, its subsequent diffusion into the water film and its adsorption (and subsequent destruction) on the cuticle itself:

$$g_{cut,wet,O3,j} = K_H P_a V_{bot} \frac{1}{1+\beta_j} \quad (4a)$$

where K_H is the Henry constant for ozone in water (1.09 10^{-4} mol m^{-3} Pa^{-1} at 25°C), P_a (Pa) denotes atmospheric pressure, V_{bot} (m s^{-1}) is the adsorption velocity of the cuticle at the bottom of the water film and $\beta_j = V_{bot}\, l_{w,j} / D_{O3,aq}$, where $D_{O3,aq}$ is the diffusivity of ozone in water (2 10^{-9} m^2 s^{-1} at 25°C).

Ozone destruction during diffusion through the water film was embedded following a similar approach as in Tuzet *et al.*(Tuzet *et al.*) for the diffusion of ozone in the apoplast, $g_{cut,wet,O3,j}$ was then derived by solving a first-order reaction-diffusion equation in the liquid film, assuming steady state:

$$g_{\mathrm{cut,wet,O3,j}} = K_{\mathrm{H}} P_{\mathrm{a}} \frac{D_{\mathrm{O3,aq}}}{d_{\mathrm{j}}} \frac{q_{\mathrm{j}} \cdot \tanh q_{\mathrm{j}} + \beta_{\mathrm{j}}}{q_{\mathrm{j}} + \beta_{\mathrm{j}} \cdot \tanh q_{\mathrm{j}}} \qquad (k_{\mathrm{j}} \neq 0) \qquad (4b)$$

where $d_j = (D_{O3,aq}/k_j)^{1/2}$ is the diffusive-to-reactive characteristic length scale in the water film, where k_j (s^{-1}) is the first-order reaction rate of ozone in the water film and $q_j = l_{w,j}/d_j$.

In a first hypothesis (H_1), we assume that the reaction rate k_j is constant. This corresponds to the situation where ozone reacts with compounds whose concentrations remain stable, regardless of the water film thickness (e.g. by evaporating at the same rate as the water film). In a second hypothesis (H_2), we assume that the quantity of reactive compounds is constant on a leaf area basis and thus gets more concentrated when the leaf dries and the water film gets thinner (e.g. soluble salts deposited at the leaf surface). In this case, the first-order reaction rate varies with $l_{w,j}$ according to:

$$k_j = V_0 / l_{w,j} \qquad (5)$$

where $V_0 = q_0 k_0$ (m s^{-1}) is a parameter proportional to the quantity of reactive compounds on the leaf surface (q_0) and their reactivity k_0.

The response of $g_{cut,wet,O3,j}$ to $l_{w,j}$ will depend on the values used for V_{bot} and k_j and whether k_j is taken constant (H_1) or proportional to $1/l_{w,j}$ (H_2), as illustrated in Figure 1. When k_j is constant, $g_{cut,wet,O3,j}$ varies from V_{bot} at low $l_{w,j}$ to $\sqrt{k_j D_{O3,aq}}$ at large $l_{w,j}$. Thus, when $V_{bot} > \sqrt{k_j D_{O3,aq}}$, $g_{cut,wet,O3,j}$ decreases with increasing $l_{w,j}$ and when $V_{bot} < \sqrt{k_j D_{O3,aq}}$ it increases with $l_{w,j}$. On the other hand, when a constant quantity of reactive compounds is considered at the leaf surface, $g_{cut,wet,O3,j}$ always decreases with increasing $l_{w,j}$. Even with $V_{bot} = 0$, large $g_{cut,wet,O3,j}$ values can be obtained at low film water thickness, provided that V_0 is large enough.

Finally, the flux of ozone was modulated by the wet fraction of leaves

$$F_{\mathrm{O3}}^{\mathrm{cut,wet}} = -\sum_{\mathrm{j}} p_{\mathrm{wet,j}} \frac{c_{\mathrm{O3a,j}}}{(g_{\mathrm{b,O3,j}})^{-1} + (g_{\mathrm{cut,wet,O3,j}})^{-1}} \qquad (6)$$

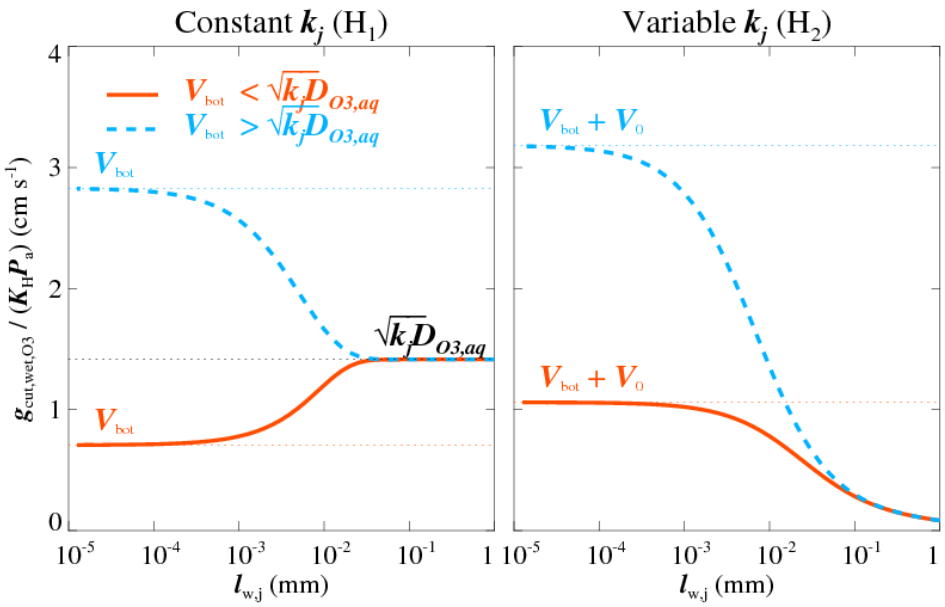

Figure 1. Normalised ozone water film conductance as a function of water film thickness (lw,j) for a constant reaction rate kj (H1; left) and variable reaction rate (H2, right). DO3,aq is the molecular diffusion constant of ozone in water, KH is the Henry constant for ozone (Pa-1), and Pa is the air pressure (Pa), and V0 is a parameter proportional to the quantity of reactive compound at the surface. The bold lines correspond to Vbot = 7.1 10-3 m s-1 ($0.5\sqrt{k_j D_{O3,aq}}$, with kj = 103 s-1) while the dotted lines to Vbot = 2.8 10-2 m s-1 ($2\sqrt{k_j D_{O3,aq}}$). V0 was set to 0.25 m s-1.

3. Tests of the new wet deposition scheme

The new ozone deposition scheme was tested against datasets collected in an agricultural field in Grignon (20 km West of Paris) over three growing seasons. This experimental site was part of the CarboEurope and NitroEurope European networks and is part of the ICOS European observation infrastructure. The site was also an intensive flux measurement site in ECLAIRE C1. The site characteristics and the selected period, from maximum vegetation development to harvest, are given in Table 1. The ozone deposition scheme was introduced into the MusiCA model for testing purposes (Ogee *et al.*, 2003). MusiCA is a multi-layer, multi-leaf, soil-vegetation-atmosphere transfer model computing the exchanges of energy, CO_2, water and their stable isotopes in the soil-vegetation-atmosphere continuum. The model considers several vegetation classes in each layer according to their light regime (sunlit or shaded), age (days or years depending on the species) and water status (wet or dry). It is a good process based model for testing the deposition scheme prior to inclusion in ESX.

Table 1**.** Main characteristics of the experimental site and measurement periods where the wet-cuticle ozone deposition parameterisation was tested.

Year	Crop type	Growth Period	Senescent period	Maximum vegetation height	Measurement height
2006	Wheat (Isengrain)	days 90-155 (31/3 to 4/6)	days 156-196 (5/6 to 15/7)	0.85m	3m
2009	Wheat (Premio)	days 90-176 (31/3 to 25/6)	days 177-212 (26/6 to 31/7)	0.86m	3.2m

2012	Wheat (Atlass/Premio)	91 to 171 (31/3 to 19/7)	172 to 216 (20/6 to 3/8)	0.75m	3m

Using $V_{bot} = 0$ and a constant reaction rate k (H1), the best agreement between modelled and observed deposition velocities was found with $k = 10^3$ s^{-1} from April (Figure 2, left panels) to June (Figure 2, middle panels). However, during senescence, a larger value of $k = 10^5$ s^{-1} gave a better agreement (Figure 2, right panels). Interestingly we were also able to match observed and modelled $V_{d,O3}$ with a variable k (hypothesis H_2) if V_0 was set to values that led to similar chemical reaction rates as in Error! Reference source not found. at mean l_w ((i.e. V_0 =0.1m s^{-1} and 10 m s^{-1} before and during senescence respectively, see Figure 2). The main differences between the two hypotheses happen at low mean water film thickness (l_w <0.1 mm), where H_2 tends to provide modelled $V_{d,O3}$ values that are greater than H_1, and usually overestimated compared to the observations (see Figure 2, e.g., on the 18th or 21st of April or 10th of June around midnight). As a consequence the comparison of modelled and versus $V_{d,O3}$ is slightly better for H_1 than for H_2, with lower RMSE values (by about 0.1 m s^{-1}) as well as greater r^2.

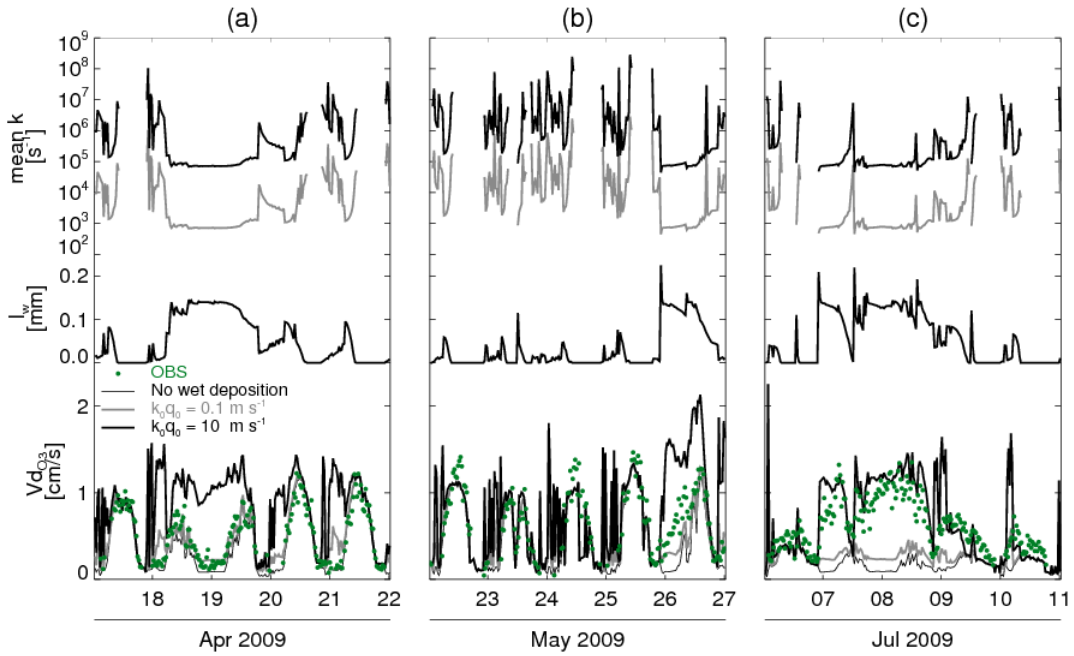

Figure 2. Time-series of mean chemical reaction rate (k, top), mean water film thickness (l_w, middle) and ozone deposition velocities ($V_{d,O3}$, low) at three different periods in 2009 (a,b,c). Observed $V_{d,O3}$ (circles). Modelled $V_{d,O3}$ are shown assuming no deposition on water film (black thin lines) or assuming deposition on the water film following the Hypothesis H2 (thick lines) with different values of a chemical compounds quantity in the water film (q_0).

4. Conclusions

This increase in O_3 deposition was well reproduced by adjusting the reaction rate of ozone in the water film to values corresponding to the reaction rate with ascorbate in the plant cells. We therefore hypothesise that during senescence, and especially when the leaves are wet, apoplastic anti-oxidants leak out to the leaf surface where they can react with ozone. The main limitation of this work resides in the validation of the water film thickness magnitude and dynamics, which is a sensitive

parameter. Efforts should be focused on measuring this term, which is not only essential for modelling ozone deposition but also other atmospheric reactive compounds. The transfer of compounds from and to the leaf through the cuticle should also be better characterised, and especially during senescence. Our hypothesis should also be tested on a range of ecosystems to check whether ozone deposition is systematically larger on wet senescing vegetation. A question also arises as to whether relatively fresh plant residues at the soil surface would also enhance ozone deposition and how this will interact with soil water. Controlled studies measuring ozone deposition to a range of senescing plants and soil organic matter composition would be desirable to generalize this study.

This module is available in fortran for inclusion into ESX.

5. References

J.A. Garland. 1977. The dry deposition of sulphur dioxide to land and water surfaces. *Proceedings of the Royal Society of London A.*, **354,** 245-268.

J. Ogee, Y. Brunet, D. Loustau, P. Berbigier & S. Delzon. 2003. MuSICA, a CO2, water and energy multilayer, multileaf pine forest model: evaluation from hourly to yearly time scales and sensitivity analysis. *Global Change Biology*, **9,** 697-717.

A.J. Rutter, K.A. Kershaw, P.C. Robins & A.J. Morton. 1971. A predictive model of rainfall interception in forests, 1. Derivation of the model from observations in a plantation of Corsican pine. *Agricultural Meteorology*, **9,** 367-384.

A. Tuzet, A. Perrier, B. Loubet & P. Cellier. 2011. Modelling ozone deposition fluxes: The relative roles of deposition and detoxification processes. *Agricultural and Forest Meteorology*, **151,** 480-492.

3. A new parameterisation of ozone deposition to bare soil

1. Estimating the surface relative humidity as a function of the heat fluxes

In the following the soil surface temperature and relative humidity are used. Using the resistance analogy, it is possible to express the surface temperature (T_{surf}) and surface concentration of water vapour ($\chi_{H2Osurf}$) at $z_{0'}$ (soil roughness height for scalar, i.e under R_b) from sensible (H) and latent heat (LE) fluxes as:

$$T_{surf} = \frac{H \cdot (R_a + R_b)}{\rho C_p} + T_a \quad (7)$$

$$\chi_{H2Osurf} = E \cdot (R_a + R_{bH2O}) + \chi_{H2Oa} \quad (8)$$

where T_a is the air temperature (°C), ρ is the air density (kg m^{-3}), C_p is the air specific heat (J kg^{-1} K^{-1}), E is the water vapour flux (kg m^{-2} s^{-1}) and χ_{H2Oa} is the air concentration of water (g m^{-3}) calculated from air relative humidity, R_a (s m^{-1}) is the aerodynamic resistance, R_b (s m^{-1}) is the quasi-laminar boundary layer resistance and R_{soil} (s m^{-1}) is the soil resistance for ozone. R_a and R_b are calculated following Garland et al. (Garland) as:

$$R_a(z) = \frac{u(z)}{u_*^2} - \frac{\Psi_H(z/L) - \Psi_M(z/L)}{k u_*} \quad (9)$$

$$R_b = (B_{St} u_*)^{-1} \quad (10)$$

where k is the von Karman's constant (0.40), B_{St} is the Stanton number (dependent of gas considered), u is the wind speed (m s^{-1}), u_* is the friction velocity (m s^{-1}) and Ψ_H and Ψ_M are height integrated similarity functions which results in the stability correction for heat and momentum respectively.
$\chi_{H2Osurf}$ allows then to calculate the surface relative humidity (RH_{surf}) at $z_{0'}$ using T_{surf} as:

$$RH_{surf} = \frac{P_{vapsurf}}{P_{sat}(T_{surf})} \times 100 \quad (11)$$

$$P_{vapsurf} = \frac{\chi_{H2Osurf} \cdot R \cdot (T_{surf} + 273.15)}{M_{H2O}} \quad (12)$$

$$P_{sat}(T_{surf}) = p \cdot \exp\left(\frac{M_{H2O} \cdot 10^{-3} \cdot L}{R} \cdot \left(\frac{1}{T_0 + 273.15} - \frac{1}{T_{surf} + 273.15}\right)\right) \quad (13)$$

where $P_{vapsurf}$ is the water vapour pressure at $z_{0'}$ (Pa), $P_{sat}(T_{surf})$ the saturation vapour pressure at T_{surf} (Pa), p the atmospheric pressure (Pa), R the universal gaz constant (J mol^{-1} k^{-1}), M_{H2O} is the molecular weight of water (g mol^{-1}), L is the latent heat of vaporisation of water (J kg^{-1}) and T_0 is the boiling temperature of water (°C).

2. A new paramétrisation of O_3 deposition velocity to bare soil

The new parameterisation of O_3 deposition was derived from experimental data in Grignon (FR). a barley harvest and consecutive ploughing and sowing of mustard. The second dataset (Period B) was collected immediately following mustard crushing, ploughing but before maize establishment and slurry incorporation of 60 kgN ha^{-1}on the 16th April, mineral nitrogen application as UAN (Urea and Ammonium Nitrate) solution on 5th May of 60 kgN ha^{-1}, and until the first maize leaves appeared, i.e. from 17th April 2008 to 10th May 2008. The third dataset (Period C) corresponded to the period from 26th September 2008 to 17th October 2008, immediately following ploughing on 25th September 2008 after maize harvest and until the first leaves of the next crop (wheat) appeared.
During each experimental period, turbulent fluxes of momentum, sensible heat, water vapour, CO_2 and ozone were measured by eddy covariance at 3.4 m height. The measuring system included a 3D sonic anemometer (R3, Gill Inc., UK), an open-path infrared absorption spectrometer for water vapour and CO_2 (IRGA 7500, LiCor, USA) and a fast-response O_3 chemiluminescent analyser (ATDD, NOAA, USA).
The empirical relationship found in Figure 6b is well fitted with the general form for soil resistance:

$$R_{soil} = R_{soil\min} \times e^{(\alpha \times RH_{surf})} \quad (14)$$

where $R_{soilmin}$ (s m^{-1}) is the soil resistance without water adsorbed at the surface (i.e. at RH_{surf} = 0%) and α is an empirical coefficient of the exponential function. The values of these two constants are given by the regression of R_{soil} vs RH_{surf} over the three datasets. The values obtained are $R_{soilmin}$ = 21.15 (± 1.01) s m^{-1} and α = 0.024 (± 0.001). In order to see the capacity of this empirical expression for R_{soil} to represent the measured deposition velocity, a modelled V_d was evaluated by combining equation (1) and (12).

Time series of measured and modelled V_d for the three datasets are shown in Fig. 7. The comparison shows that the model reproduces the measurements quite well, for both daily and day-to-day variations, for period A (Fig. 7a) and period C (Fig. 7c). During these two periods, the model underestimates the measurements by only 4 (± 3) % and 14 (± 9) % for 2007 and late 2008 respectively. Although the empirical relationship found in Figure 6 worked on all datasets, the agreement in period B was the poorest (the scatter was the largest for that period; R^2 = 0.40 for period B whereas R^2 = 0.65 and 0.57 for periods A and C respectively). In order to understand this discrepancy, the potential role of reactions between NO and O_3 is investigated in the following.

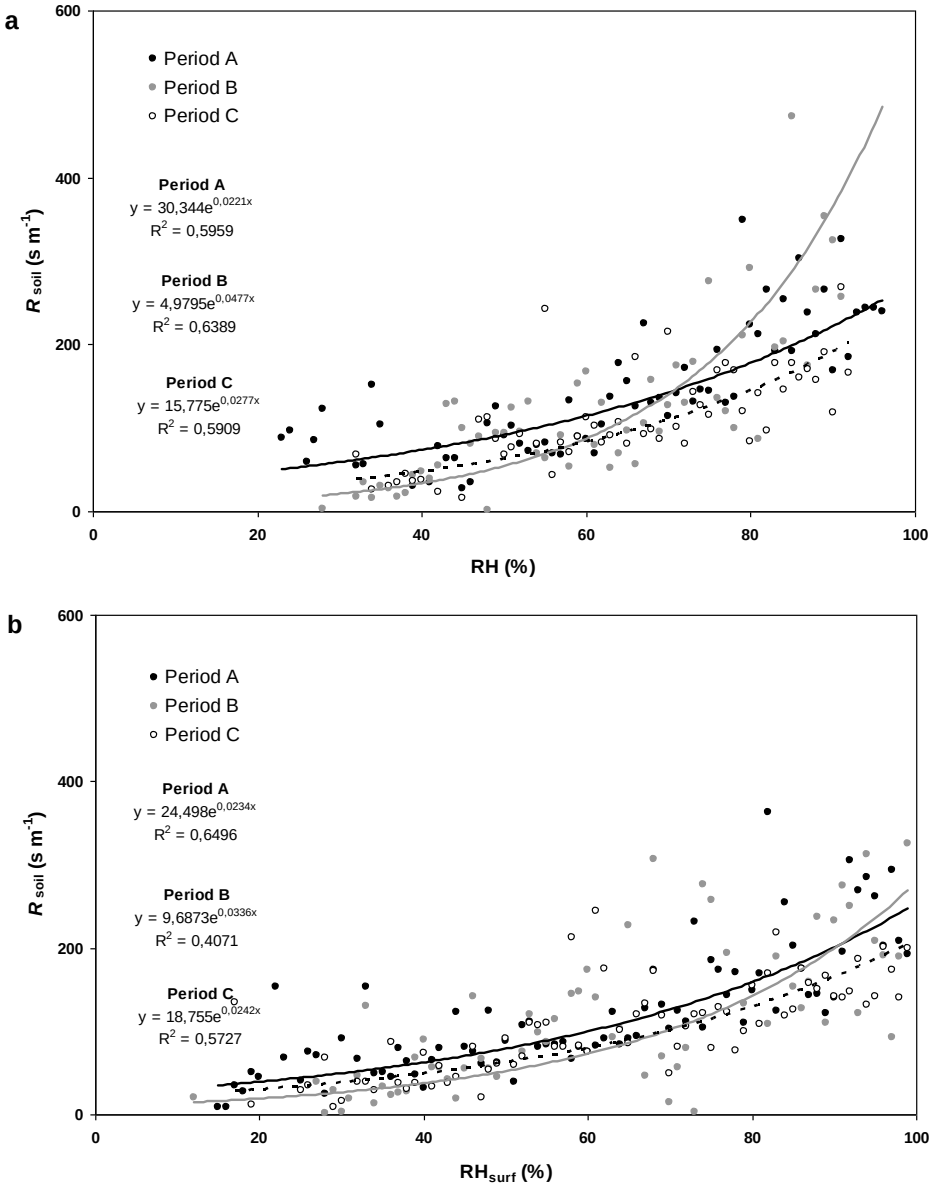

Figure 3. Soil resistance (R_{soil}) as a function of (a) air relative humidity (RH) and (b) surface relative humidity (RH_{surf}). Black, grey and open symbols are block averaged data from Period A, B and C respectively. Black, grey and dotted lines are regressions for data from Period A, Period B and Period C respectively. The range used for block averages is 1%. Only data for $u_* > 0.2$ m s-1 were used.

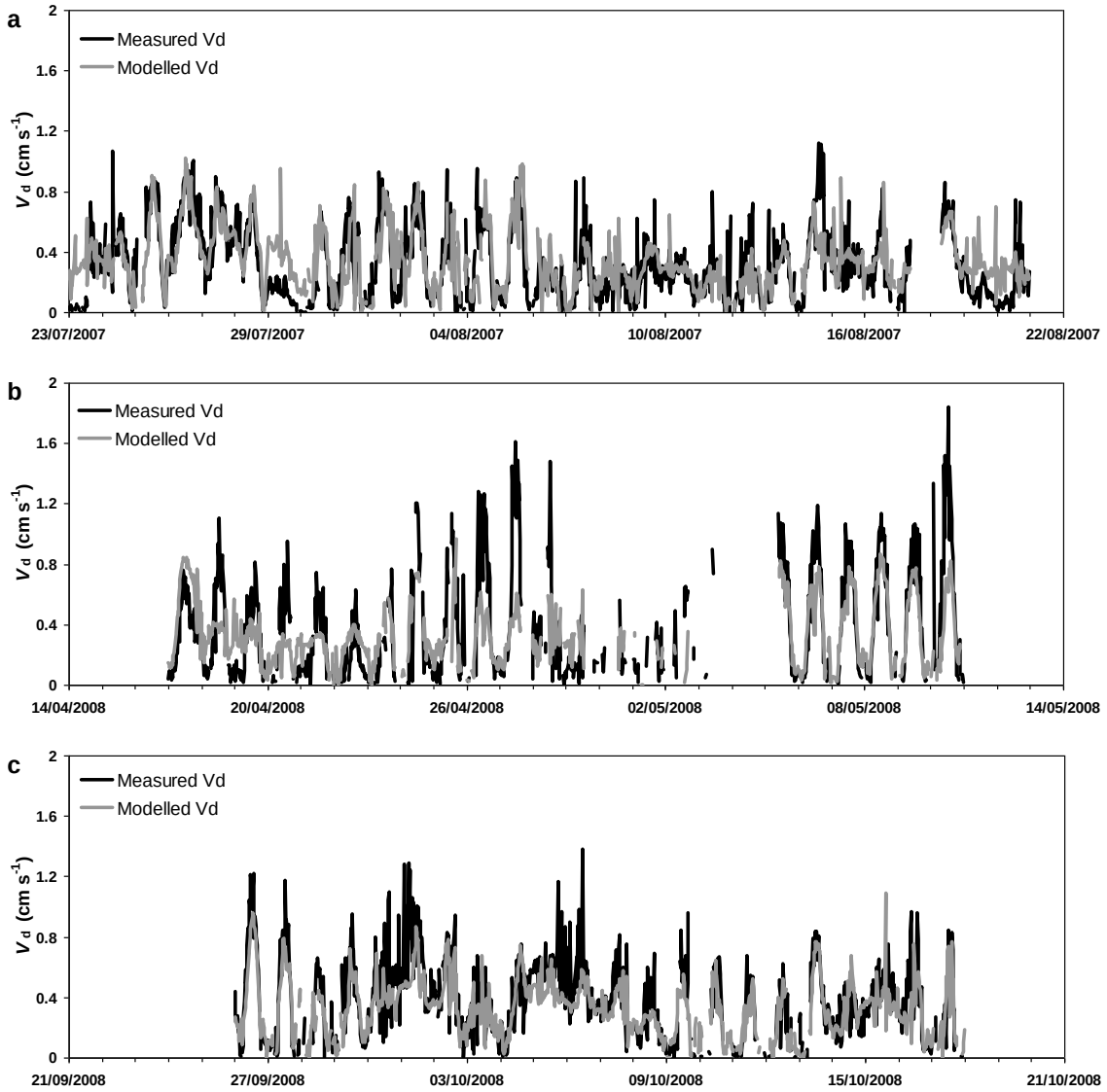

Figure 7. Time series of ozone deposition velocity (V_d) from (a) Period A, (b) Period B and (c) Period C. Black and grey lines are respectively measured and modelled V_d.

3. Conclusions

A new parameterisation of soil resistance as a function of surface relative humidity is proposed, introducing a minimal soil resistance and an empirical exponential term. The comparison of measured and modelled values over the three datasets shows a good agreement when there is no soil NO emissions. This derivation was obtained over one soil type. Studying the effect of soil properties, as porosity, organic matter content, acidity, on R_{soil} is a prerequisite prior to generalising the results found here to other soil types and conditions. Additional datasets from the Eclaire experimental sites will allow generalising this result by providing a range of conditions to tabulate $R_{soil\ min}$ and α.